International Journal of Engineering and Technology sciences (IJETS) 2 (3): 223-242, 2014
ISSN 2289-4152
© Academic Research Online Publisher

Research Article

Modelling and CFD Simulation of Hydrodynamics and Mass Transfer in a Miniature Bubble Column Bioreactor

Soheila Kheradmandnia, Seyyed Mohammad Mousavi *, Sameereh Hashemi-Najafabadi **, Seyed Abbas Shojaosadati

Biotechnology Group, Chemical Engineering Faculty, Tarbiat Modares University, P.O.Box: 14115-114, Tehran, Iran

* Corresponding author: Biotechnology Group, Chemical Engineering Faculty, Tarbiat Modares University, P.O.Box: 14115-114, Tehran, Iran, Tel.: +98-21-82884917; Fax: +98-21-82884931
E-mail address: mousavi_m@modares.ac.ir

** Corresponding author: Biotechnology Group, Chemical Engineering Faculty, Tarbiat Modares University, P.O.Box: 14115-114, Tehran, Iran, Tel.: +98-21-82884384; Fax: +98-21-82884931
E-mail address: s.hashemi@modares.ac.ir

A b s t r a c t

Keywords:

Computational fluid dynamics (CFD), Flow pattern, Miniature bubble column bioreactor(MBCR), Volumetric mass transfer coefficient ($K_L a$).

Computational fluid dynamics (CFD) was used to study a 3D simulation of hydrodynamics and mass transfer in a miniature bubble column bioreactor (MBCR). The ability of a two-fluid phase model to predict flow behaviour was studied by applying the laminar and turbulence models. The volumetric mass transfer coefficient (K_La) was predicted at different superficial gas velocities and sparger pore sizes. The simulation results of K_La showed a good agreement with the experimental data in a 30 μm sparger pore size. A similar behaviour was observed in the liquid circulation, gas distribution and their relation in the MBCR like as large scale bubble columns. Increasing the superficial gas velocity led to an increase in the liquid circulation near the walls, followed by an increase of the gas holdup and K_La. Decreasing the pore size of sparger produced smaller bubbles which resulted in increased gas holdup and K_La. Linear relation between the superficial gas velocity and interfacial area was investigated as the same as a short bubble columns. Observation of the similar behaviour in the hydrodynamic characteristics of traditional and miniature scales of the bubble columns may encourage the researchers to develop the MBCRs in the high throughput processes.

Accepted:26 April2014
© Academic Research Online Publisher. All rights reserved.

Nomenclature

General Symbols

a	Interfacial area (m^{-1})	Re_b	Bubble Reynolds number
C_D	Drag force coefficient	$\mathrm{Re}_{0L}=\frac{4Q\rho_L}{\pi d_0 \mu_L}$	Modified sparger Reynolds number
C_L	Concentration of dissolved oxygen ($Kg.m^{-3}$)	S	Interphase mass transfer ($Kg.m^{-3}s^{-1}$)
C_L^*	Saturation concentration of dissolved oxygen ($Kg.m^{-3}$)	$Sc=\frac{\mu_L}{\rho_L D}$	Schmitt number
$\overline{C}_L$	Steady state concentration of dissolved oxygen ($Kg.m^{-3}$)	Sh	Sherwood number
C_{lift}	Lift force coefficient	t	Time (s)
C_μ	Coefficient for turbulence viscosity	u	Velocity ($m.s^{-1}$)
$C_{1\varepsilon}, C_{2\varepsilon}$	Constants in k–ε model		
D	Diffusion coefficient ($m^2.s^{-1}$)		
d_0	Sparger pore size (m, μm)	**Greek Symbols**	
d_b	Average bubble diameter (m)	α	Phase volume fraction
Eo	Eötvös number	μ_{eff}	Effective viscosity ($pa.s^{-1}$)
F	Interfacial force between liquid and gas phase ($N.m^{-3}$)	ρ	Density ($kg.m^{-3}$)
F_D	Drag force ($N.m^{-3}$)	ε	Turbulence dissipation rate of specific phase ($m^2.s^{-3}$)
F_{Lift}	Lift force ($N.m^{-3}$)	σ	Surface tension ($N.m^{-1}$)
$Fr_0=\frac{Q^2}{g\,d_0}$	Sparger Froude number		
g	Gravitational acceleration (ms^{-2})	**Subscripts**	
k	Turbulence kinetic energy of specific phase ($m^2.s^{-2}$)	b	Bubble
K_L	Liquid mass transfer coefficient (ms^{-1})	D	Drag
OUR	Oxygen Uptake Rate ($Kg.m^{-3}s^{-1}$)	G	Gas
P	Pressure (pa)	k	Phase
		L	Liquid

1. Introduction

In recent years, bioprocess development such as screening and optimization has been performed at small scale systems [1]. Scaling down the volume of the bioreactors, performing parallel bioprocesses and on-line monitoring the experiments create a good opportunity for saving in time, materials and labor intensity [2]. Ability of the miniature bioreactors to examine a wide range of experimental conditions and select the optimized conditions, makes them as high-throughput systems for bioprocess development [3]. Parallel MBCRs are one of the suitable candidates for medium or strain improvement and early-stage process development beside the other small scale systems [4]. Similar to laboratory and large scale bubble columns, miniature columns are mechanically simple and their final

design cost is less than stirred tanks. They can be easily instrumented, automated and characterized [5, 6].

In the bubble column bioreactors, operation is performed via contact between gas and liquid phase. Aeration and mixing are achieved by gas sparging from the bottom of the column. Sparger type, superficial gas velocity and bubble size distribution as the main factors affect the transport phenomena in these devices [7]. Sparger type and gas flow rate affect the size and behavior of the released bubbles from the sparger, gas hold up, fluid mixing and oxygen transfer rate [8]. Despite the simple design, the flow behaviour is complicated in the bubble columns. Three flow regimes occur in these columns depending on the inlet gas flow rate and column diameter [9]. At low superficial gas velocities (< 0.05 $m.s^{-1}$), homogeneous or bubbly flow is dominant in the column. In the homogeneous regime, bubbles are small with a uniform distribution. Turbulence and bubble coalescing or breaking can be neglected. Liquid circulation is small and finally the radial profiles of gas hold up and liquid velocity is obtained. By increasing the superficial gas velocity, heterogeneous condition is dominant in the system. In a heterogeneous regime, the bubble swarming occurs which is directed towards the wall of the bioreactor. Large bubbles are formed by coalescence depending on the column diameter. The recirculation rate in the vessel is increased, extensively. Hold up and liquid velocity magnitude are at the maximum values at the center of the column and their profiles are parabolic with the sharp peak. The third regime is the intermediate regime that is called transition flow regime. This regime exists between the homogeneous and heterogeneous flows. The major phenomenon in the transition flow is the coalescence and formation of larger bubbles rather than homogeneous flow [6].

Performance of the bubble column reactors is determined by the flow regime and mass and momentum transfer in the column [10]. Over the last few years, computational fluid dynamics (CFD) have found a widespread application to describe the flow hydrodynamics and mass transfer in many bioreactors, especially bubble columns [11, 12]. However, modelling of transport phenomena in the miniature bioreactors is still rare. Lamping et al., successfully modelled liquid and gas speed, energy dissipation rate, gas hold up and $K_L a$ in a miniature stirred tank bioreactor by CFD simulations [13]. Zhang et al., applied CFD to a single well of both 24-well and 96-well microtiter plates [14]. The liquid velocity, gas liquid interface, power consumption and energy dissipation rate were predicted in a well of microtiter plate during orbital shaking. Rihani et al., used CFD in a milli torus reactor with $k-\varepsilon$ turbulent model to simulate flow pattern, turbulence and gas hold up profiles [15]. There is no report on the CFD simulation of miniature bubble column bioreactors in literatures. Therefore, to observe the potential of computational techniques in prediction of flow and mass transfer in the small scale bioreactors, hydrodynamics and $K_L a$ have been simulated in the MBCR with 2 mL working

volume. Possible similarities and differences between the large and small scales of the bubble columns are also investigated. To validate the model, results have been compared against the experimental data presented by Doig et al., [16].

2. Experimental procedures

2.1. Geometry and grid of the miniature column

To simulate the miniature bubble column, one small scale column with a cross section of 17 × 8 ($\times 10^{-6}$ m^2) and a height of 15 ($\times 10^{-3}$ m) was constructed and meshed with Gambit 2.3 (Fluent Inc., USA). The bottom surface in the geometry was assumed as a uniform plate for gas sparging and no holes were considered in the gambit model. The effect of the pore size in different sintered glass spargers was indirectly applied on defined bubble diameter in the model.

The geometry was meshed by tetra hybrid elements. The mesh spacing was set to 0.7 and 1×10^5 tetrahedral cells were created. Fig.1 (a, b) shows a schematic of the geometry. Fig.1 (c, d) displays the meshed surface at different cutting planes. The geometry is exactly as the same as the bioreactor used by Doig et al., [16].

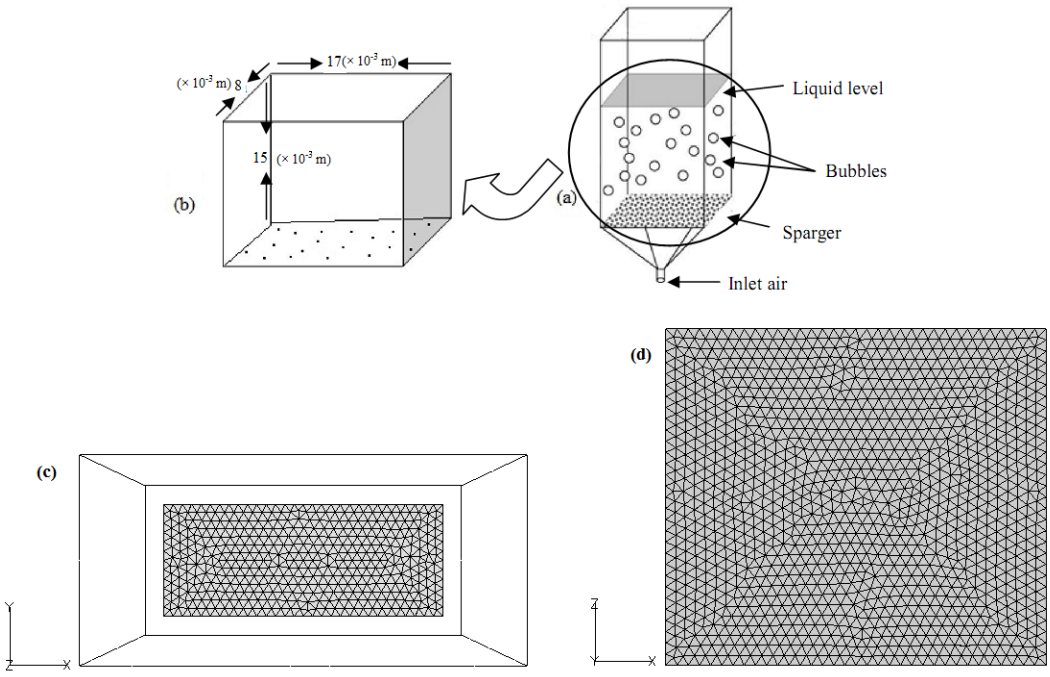


Fig. 1: The schematic (a) and dimensions (b) of the miniature bubble column used in the simulations. c: Grids for the inlet (xy surface); d: Grids for the height (z direction).

2.2. Model equations

The Eulerian two phase model was used to simulate dispersion of gas in the liquid. The mass and momentum balance equations were written separately for the liquid phase as continues phase and the air bubbles as disperse phase. Liquid phase properties were considered as the same as water. The continuity equation is written as Eq. (1).

$$\frac{\partial(\alpha_k \rho_k)}{\partial t} + \nabla.(\alpha_k \rho_k u_k) = 0 \qquad (1)$$

which α_k is the volume fraction, ρ_k is the density, u_k is the average velocity for the k^{th} phase [17, 18]. The momentum equation for each phase is written as Eq. (2).

$$\frac{\partial(\alpha_k u_k \rho_k)}{\partial t} + \nabla.(\alpha_k \rho_k u_k u_k) = -\alpha_k \nabla P + \alpha_k \rho_k g + \nabla[\mu_k \nabla.(\rho_k u)] + F \qquad (2)$$

The right term of Eq. (2) describes the entire forces acting on the phase k : pressure gradient, gravity, viscous stress and F is the interfacial force between the liquid and gas phases such as drag, lift and virtual mass forces. In the present analysis, the virtual mass force was ignored while drag and lift forces were included to the model. Eq. (3) is solved for oxygen transport.

$$\frac{\partial(\alpha_k C_k \rho_k)}{\partial t} + \nabla.(\alpha_k \rho_k C_k u_k - D_k \alpha_k \rho_k \nabla C_k) = S_k \qquad (3)$$

C is O_2 concentration, D is O_2 diffusion coefficient in the water and S_k is the flux of oxygen for the k^{th} phase. D with the value of 2.4×10^{-9} $m^2.s^{-1}$ is applied to the model at 30 °C.

The flux of oxygen from the air bubbles (gas phase) to the water (liquid phase) is defined as Eq. (4).

$$S_k = S_{GL} = K_L a (C_L^* - C_L) \qquad (4)$$

Here, C_L and C_L^* are the concentration and saturation concentration of dissolved oxygen in the liquid phase, respectively. C_L^* for dissolved oxygen in pure water at 30°C has been reported as 8×10^{-3} ($Kg.m^{-3}$) [19].

In a well mixed water phase, the rate of C_L changes is equal to the rate of oxygen transfer from the air to the water minus the rate of oxygen uptake (OUR) by the microorganisms [19, 20].

$$(1-\alpha_G)\frac{dC_L}{dt} = K_L a (C_L^* - C_L) - OUR \qquad (5)$$

where, α_G is the gas volume fraction in the liquid phase. In the steady state condition, C_L reaches to the steady state value of $\overline{C}_L$ and OUR can be calculated by Eq. (6).

$$OUR = K_L a (C_L^* - \overline{C}_L) \qquad (6)$$

Replacement of OUR in Eq. (5) with Eq. (6) leads to Eq. (7).

$$(1-\alpha_G)\frac{dC_L}{dt} = K_L a (\overline{C}_L - C_L) \qquad (7)$$

Integrating Eq. (7) from initial condition ($t=0, C_L=0$) to any time is led to Eq. (8).

$$\frac{C_L}{\overline{C}_L} = 1-\exp(-\frac{K_L a}{1-\alpha_G}t) \qquad (8)$$

while $\overline{C}_L$ is a fraction of C_L^*. At the stationary phase of microorganism growth, $\overline{C}_L$ approaches to C_L^* and Eq. (8) can be rewritten as Eq. (9).

$$\frac{C_L}{C^*_L} = 1-\exp(-\frac{K_L a}{1-\alpha_G}t) \qquad (9)$$

Finally, S_{GL} is calculated by substituting C_L from Eq. (9) into Eq. (4).

$$S_{GL} = K_L a\, C_L^* \exp(-\frac{K_L a}{1-\alpha_G}t) \qquad (10)$$

The interphase momentum transfer between two phases is given by Eq. (11).

$$F_D = \frac{3}{4} C_D \alpha_G \rho_L \frac{1}{d_b} |u_G - u_L| (u_G - u_L) \qquad (11)$$

α_G is the volume fraction of gas phase as mentioned before, d_b is the average bubble diameter in the bioreactor and $(u_G - u_L)$ is the slip velocity between the liquid and gas phases [17].

C_D, is drag coefficient which depends on the flow around the bubbles. It is calculated according to model of Schiller and Naumann (Eq. 12):

$$C_D = \begin{cases} \frac{24}{\mathrm{Re}_b}(1+0.15\mathrm{Re}_b^{0.687}) & \mathrm{Re}_b \le 1000 \\ 0.44 & \mathrm{Re}_b > 1000 \end{cases} \qquad (12)$$

Re_b is bubble Reynolds number. The surface tension (σ), has a value of 0.071 ($\mathrm{N.m^{-1}}$) for water and air at 30 °C. Lift forces is included in the model to consider the effect of the interaction between the bubbles and shear stress. The lift force is given by Eq. (13).

$$F_{Lift} = C_{lift}\,\alpha_G\,\rho_L\,(u_G - u_L)\times\nabla u_L \qquad (13)$$

The lift force coefficient (C_{lift}) which was applied to the model, had a value of 0.5 [21]. The other needed parameters such as bubble rising velocity (u_b) can be determined using the average bubble diameter (d_b) and the liquid properties. Mandleson equation [22] was used to calculate u_b in $\mathrm{Re}_b > 1$ according to Eq (14).

$$u_b = \left(\frac{2\sigma}{\rho_L d_b} + \frac{g\,d_b}{2}\right)^{0.5} \qquad (14)$$

Bubbles in the column assumed to include both single and chains of touching bubbles. Thus, the constant bubble diameter employed in the simulations was the average of single bubbles and chain of bubbles. For single bubbles which are distributed in the water, d_b can be predicted from the balance of buoyancy and surface tension [22] via Eq. (15).

$$d_b = \left[\frac{6\sigma d_0}{g\,(\rho_L - \rho_G)}\right]^{(1/3)} \qquad (15)$$

The bubble diameter in this study varied from 0.7 to 1.2 ($\times 10^{-3}$ m), due to the sparger pore sizes (d_0).

In the conditions that bubble chaining prevails in the column, d_b is calculated from Eq. (16) [22].

$$d_b = 3.23\,d_0\,\mathrm{Re}_{0L}^{-0.1}\,Fr_0^{0.21} \qquad (16)$$

The chain of bubbles has been reported by other researchers for a miniature scale bubble column with the sparger pore size of 10 to 100 ($\times 10^{-6}$ m) [16]. Bubble Reynolds number (Re_b), is calculated as Eq. (17) [22].

$$\mathrm{Re}_b = \frac{u_b d_b}{\mu_L} \qquad (17)$$

Re_b, varied from 61 to 196 for intermediate gas flow rates, different bubble sizes and bubble rising velocities which were applied in the simulations [16].

Hydrodynamics condition for the bubble Reynolds number in the range of 61 to 196 cannot be presumed as a fully turbulent or creeping flow [16]. According to this assumption, the laminar viscous model was studied in some primary simulations and then the $k-\varepsilon$ turbulence model was also used in this work to estimate the turbulent effects.

The turbulent effects in the liquid phase is neglected in the laminar model and the effective viscosity is equal to the effective laminar viscosity of the gas liquid mixture (Eq. (18)) [23].

$$\mu_{eff} = \mu_L (1+2.5\alpha_G) \approx \mu_L \qquad (18)$$

In the $k-\varepsilon$ turbulence framework, the effective eddy viscosity is shown as Eq. (19).

$$\mu_{eff} = C_\mu \rho_L \frac{k^2}{\varepsilon} \qquad (19)$$

k is the turbulent kinetic energy and ε is its dissipation rate. RNG $k-\varepsilon$ method has been used in this study to account the effect of entire scales of motion, especially small scales in the turbulent diffusion [24]. In RNG approach of $k-\varepsilon$ model, for primary phase (liquid phase), C_μ = 0.0845, $C_{1\varepsilon}$ = 1.42 and $C_{2\varepsilon}$ = 1.68 were used as model constants [25]. No turbulence model was included in dispersed phase. The meshes were enough fine to consider the effects of turbulence near the bioreactor walls and standard wall functions with no further treatment was applied to the model.

2.3. Volumetric mass transfer coefficient ($K_L a$) prediction

$K_L a$ is the product of liquid mass transfer coefficient (K_L) and interfacial area (a).

The Sherwood number is used to calculate K_L [16].

$$Sh = \frac{K_L d_b}{D} = 0.5 \mathrm{Re}_b^{1/2} Sc^{1/3} \quad (200 < \mathrm{Re}_b < 4000) \qquad (20)$$

Diffusion coefficient of O_2 in the water (D) with the value of 2.4×10^{-9} $m^2.s^{-1}$ is applied to the model at 30 °C. The interfacial area (a) is given as a function of volume fraction of gas phase (gas hold-up: α_G) and the average bubble diameter (d_b), according to Eq. (21) [11].

$$a = \frac{6\alpha_G}{d_b} \qquad (21)$$

2.4. Numerical implementation

2.4.1. CFD model set up

Fluent as a commercial code was used to solve three dimensional governing equations. FLUENT 6.3 installed in a supercomputer system with two processors (each processor contained 12 cores) and 32 GB available RAM. The CFD model was solved with parallelization technique that has been described in detail in the Fluent user guide [25]. The Eulerian two phase method, both of laminar and turbulent flow regimes and unsteady state condition were also included in the model. The air was selected as a unit component in the model. Thus, to consider the oxygen transfer from the air to the water, oxygen concentration was expressed according to the $K_L a$ parameter. A user define function (UDF) was implemented to the software to calculate oxygen concentration, $K_L a$ and S_{GL} using the equations discussed in sections 2.2 and 2.3. Unsteady state formulation and pressure-velocity coupling were set to the first-order implicit and phase-coupled SIMPLE respectively. First-order upwind was chosen for momentum, volume fraction and turbulent parameters. Under-relaxation factors for pressure, momentum, volume fraction, turbulent kinetic energy, turbulent dissipation rate and turbulent viscosity were set to 0.5, 0.7, 0.5, 0.7, 0.7 and 0.7, respectively. Time step and convergence criterion for each scale residual component were specified as 1×10^{-4} through the simulation. $K_L a$ was obtained when the simulations reached to steady state and total gas hold up in the column remained at a constant level.

2.4.2. Boundary conditions

The bottom plate of the column was modelled as a uniform gas inlet. The inlet gas velocity was equal to the superficial gas velocity to consider the existence of many supposed pores on the plate.

The pressure outlet was chosen for outlet and no-slip boundary condition was applied to the walls. The turbulence intensity for the boundary conditions was set at 0.05% to achieve low turbulence system [25] which was near the laminar conditions.

3. Results and Discussion

3.1. Choosing the suitable viscous model

Homogeneous flow behavior is dominant in the columns with the small diameter and low superficial gas velocity [5, 26]. Therefore, at the first step, the laminar (homogeneous) flow regime was considered in the model. By applying the laminar model the characteristics of a turbulent regime such

as sharp peak of gas hold up in the center line was observed unexpectedly (results have not been shown). It showed that this model had low ability to predict reasonable results for the simulations. Other researchers have also reported the same heterogeneous behaviour when they used the laminar model in simulation of laboratory scale bubble columns [27, 28]. Sokolichin et al., showed that by increasing the grid refinement in their reactor with laminar model, convergence in the solution was not gained and the number of circulation cells grows continuously. Grid dependency of the results is not reliable. Therefore, they studied $k-\varepsilon$ model to apply the effect of small eddies and found that in 2D version of $k-\varepsilon$ model, the grid independent solution was achieved but the dynamic nature of flow was not reproduced. According to their investigations, the experimental data were in the agreement with the results of 3D turbulent model [23]. 2D and 3D versions of $k-\varepsilon$ model for simulating the systems with low Reynolds number were used also by other researchers. For example Mudde et al., observed the steady state solution in a 2D simulation of their bubble column, but turbulent viscosity was high and the bubble plume was attached to the wall. It was caused by overestimation of the turbulent viscosity. At the next step, using a 3D simulation, the small liquid circulation was observed and the flow approached to the transient regime [29].

However some studies neglected the effect of virtual mass or lift forces in the simulation of the bubble columns [29-31], but others studied the effect of these interfacial forces on the stability and reliability of the hydrodynamic simulations in the bubble columns. Delnoij et al., applied drag, lift and virtual mass forces to simulate the hydrodynamics behaviour of a laminar flow in a bubble column [32]. In the simulated flow profiles of a bubble coumn studied by Monahan et al., all the interfacial forces had significant role [21]. Silva et al., studied the effect of interfacial forces and turbulence models in a bubble column to evaluate the flow pattern in the heterogeneous and homogeneous regimes [33].

The present work was followed by a 3D version of "RNG" $k-\varepsilon$ turbulence model to consider the effect of turbulence formed and spread by small eddies in low Reynolds number. Drag and lift forces were added to the model and the virtual mass force was neglected to avoid the instability of the solution.

3.2. The effect of grid size on the simulation results

For checking the grid independency, three different grids were used. The mesh spacing was set to 1.0 for the first grid as a coarse grid and 6×10^4 tetrahedral elements were created. The second grid was finer and contained 1×10^5 tetrahedral elements with 0.7 mesh spacing. The third grid was the finest one with 0.5 mesh spacing and 2×10^5 tetrahedral elements. The grid independency checking was done

at a constant sparger pore size of 30 μm and superficial gas velocity of 0.004 $m.s^{-1}$. The results of gas volume fraction as well as the liquid and gas velocities were recorded for all 3 cases in 5 seconds simulating. In this point the system reached to the stabilization. Total gas hold up and velocity profiles reached to a constant level and no significant changing was observed during the further iterations. The comparison of the calculated data with different grid sizes has been depicted in Table 1.

Table 1: Grid independency check.

Case number	Number of nodes	Grid Size	air volume fraction	gas velocity ($m.s^{-1}$)	liquid velocity ($m.s^{-1}$)	Time (s)
1	11720	60331	0.034	0.070	0.021	5
2	20008	105905	0.034	0.070	0.018	5
3	40470	220071	0.035	0.070	0.019	5

Preliminary calculations showed the same solution for all grids. There was no significant difference between the results of gas volume fraction and velocity. Since the results of medium and fine grids are close together, the medium grid was chosen for further simulations and all the results were investigated in 5 s simulating.

3.3. The effect of superficial gas velocity on the liquid velocity

Fig. 2(a-d) has displays the liquid velocity vectors at the x-z plane. Contours and vectors were obtained for the column with a 30 μm sparger pore size in different superficial gas velocities. The liquid phase was moved upward via the bubbles. Because of zero net liquid flow in the column, it must recircle downwards. The liquid velocity contours showed the maximum upward motion in the center of the column. Small scale of the bioreactor caused to direct the liquid downward near the walls which resulted in a liquid circulation and the increase of gas hold up in these regions. As expected, the higher superficial gas velocity induced the higher circulation and back mixing in the liquid phase.

Fig. 3(a, b) shows the stream lines of the liquid and bubbles in the simulated MBCR. The liquid stream lines (Fig. 3a) clearly presented liquid flow upward in the center-line and downward near the walls causing to produce two circulation zones in the columns. The bubble stream lines moved up directly in the central core, but near the walls the streams were pushed to the higher parts of the walls via liquid circulation (Fig. 3b).

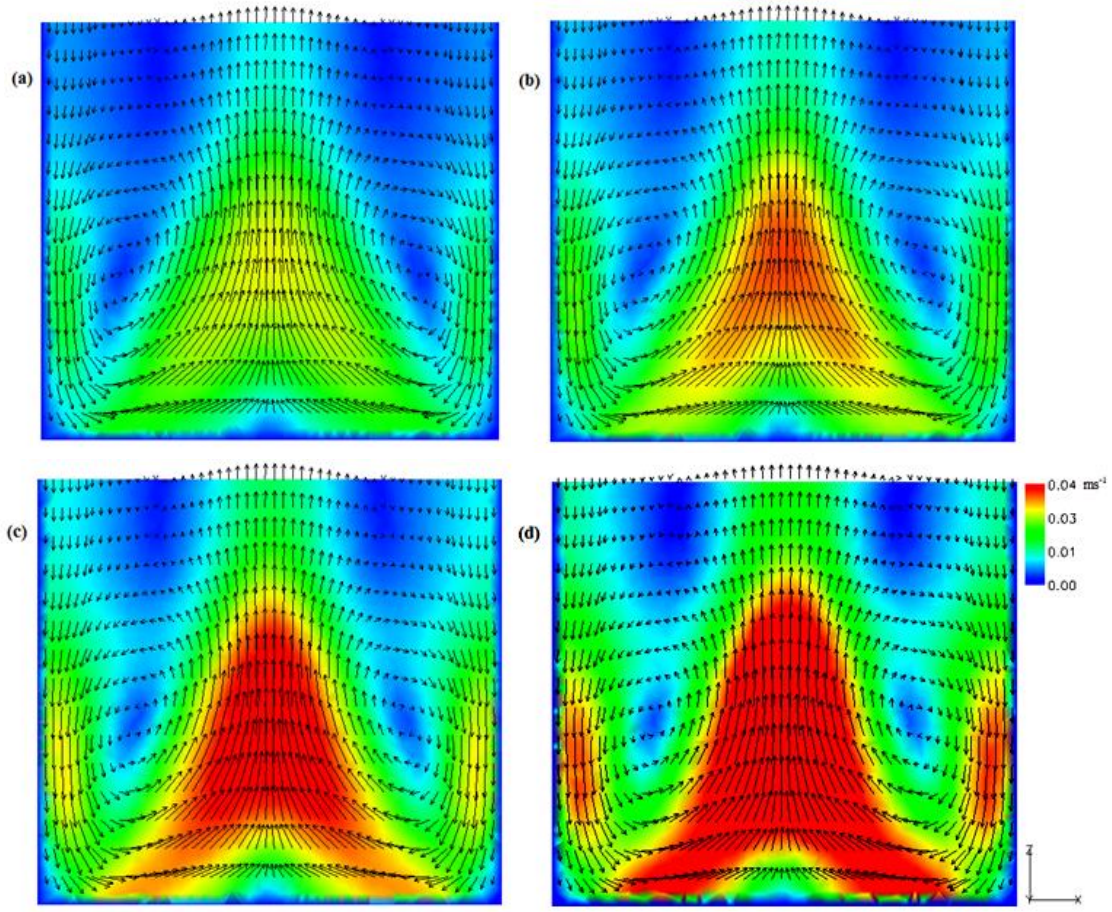


Fig. 2: The liquid velocity contours and vectors at the central x-z plane in 5 s simulating and different superficial gas velocities; a, b, c and d are 0.0015, 0.002, 0.003 and 0.004 $m.s^{-1}$ respectively.

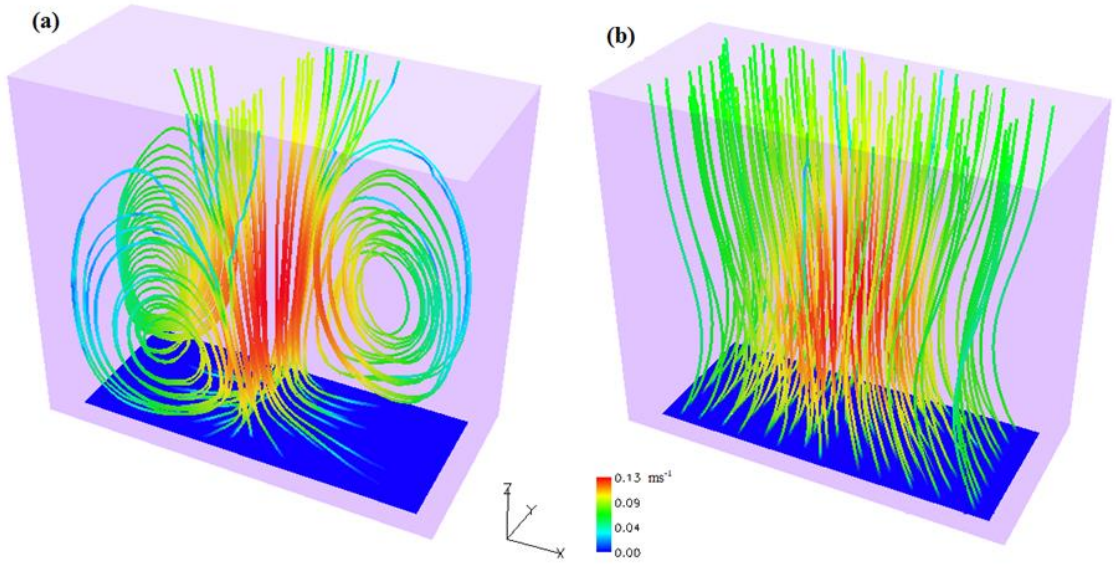


Fig. 3: Stream lines at the column; a: liquid streams line b: bubble streams line at superficial gas velocity of 0.004 $m.s^{-1}$, sparger pore size of 30 μm and 5 s simulating.

This flow behaviour was also investigated by Delnoij et al., for simulating a short bubble column with cross section of 0.175×0.175 m^2 and the ratio of height to diameter (aspect ratio) smaller than 1.0 [34]. For larger bubble columns with aspect ratio more than 1.0, the flow field changed to a more complex with s-shaped path through the column or shifted from left to right and vise versa at fully turbulent regime [35, 36].

3.4. The effect of superficial gas velocity and average bubble diameter on the gas hold up

Local gas hold up distribution has been shown in different heights of the MBCR (Fig. 4(a-d)) and different superficial gas velocities. The parabolic gas hold up profiles can be observed according to Fig. (4). Maximum and minimum values of the air fraction were observed in the center region and near the walls, respectively.

Gas hold up profiles and the liquid circulation were interrelated. By increasing the superficial gas velocity, more bubbles travelled from the center to the walls by liquid circulation. It reduced the uniform distribution of the gas in the column and produced the steeper gas hold up profiles than low superficial gas velocities. Thus two peaks were observed at higher heights of the column (h/H= 0.75) when the superficial gas velocity was greater than 0.0015 $m.s^{-1}$. Gas hold up profile in 0.0015 $m.s^{-1}$ superficial gas velocity was relatively flat at different heights of the column.

Increasing the superficial gas velocity resulted in the increase of the bubble diameter from 0.56 to 0.63 ($\times 10^{-3}$ m) and consequently the decrease of bubble rising velocity from 0.51 to 0.48 $m.s^{-1}$. However bubble rising velocities were slightly changed due to the small size of the bubbles, but producing the bubbles with larger size resulted in increased gas hold up in the MBCR by increasing superficial gas velocity.

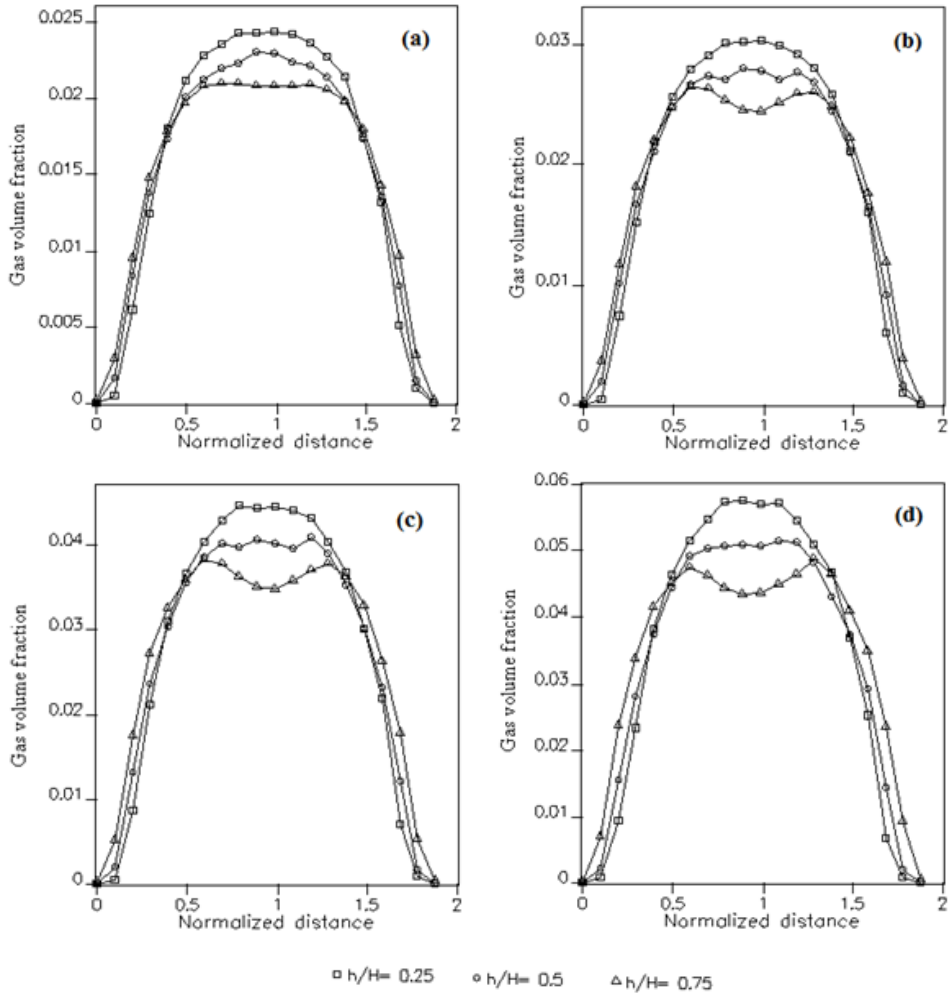


Fig. 4: Gas volume fraction vs. normalized distance for the various axial heights in 5 s simulating. Superficial gas velocity at a, b, c, d is 0.0015, 0.002, 0.003 and 0.004 $m.s^{-1}$, respectively.

In the MBCR simulated in this study the height to diameter ratio is low. Thus, as the same as other short bubble columns, the bubble coalescence and break up would not be strongly affected by the column height at low superficial gas velocities. In a short bubble column gas hold up and the interfacial area were proportional to the superficial gas velocity. Gopal et al., reported the linear relation between the interfacial area and superficial gas velocity for a column with aspect ratio of 1.0 and diameter of 0.2 m [37]. Ravinath et al., investigated the increased of gas hold up to a maximum value in the aspect ratio of 1.0 and decrease of it at the higher aspect ratios in a bubble column with multipoint sparger. Their observation at higher aspect ratios was related to coalescence of the bubbles and producing the equilibrium bubble size [38].

Linear relationship between the interfacial area and superficial gas velocity was also observed in the simulation of MBCR with different sparger pore size (Fig. (5)).

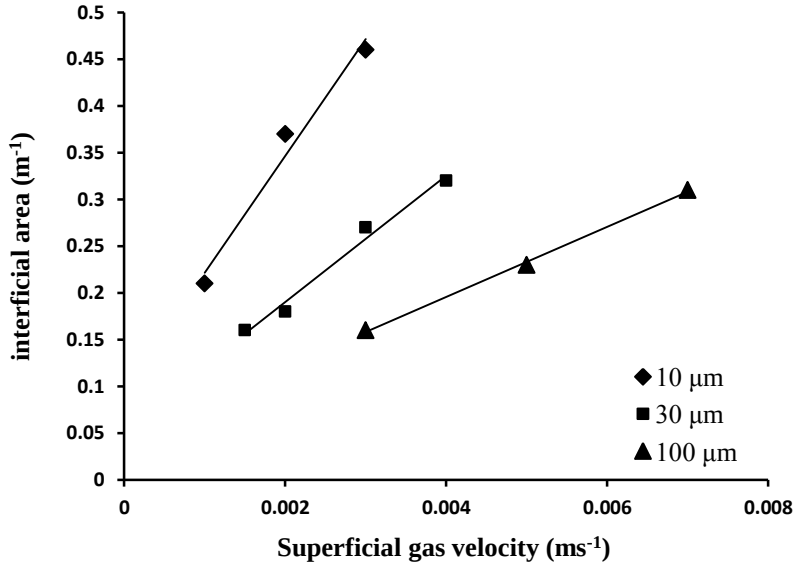


Fig. 5: Linear relation between interfacial area and superficial gas velocity for different sparger pore sizes.

3.5. The effect of sparger pore size on the liquid velocity and the gas hold up

According to the literature, the multipoint sparger obtains higher gas hold up rather than single nozzle gas spargers [17, 39, 40]. Higher value of gas hold up and interfacial area were obtained in the column with the uniform sparged gas at the bottom. In a tall and large bubble column, type and design of the gas sparger is not critical in the turbulent flow [6, 37]. But in a short bubble column gas sparger design significantly affects the performance of the column [8, 38]. Sintered glass sparger with different pore size used in this study to simulate the liquid circulation and gas hold up profiles in the MBCR.

Liquid velocity graphs at *z* direction and hold up profiles have been shown in Fig. 6(a) and Fig. 6(b), respectively. Graphs represent the radial velocity profiles with a maximum value in the center. Two circulation zones and therefore, two points with zero velocity between upward and downward were also observed for all spargers. Decreasing the sparger pore size produced the small bubbles which led to increase the bubble rising velocity and liquid velocity in the center of the column. It introduced the stronger liquid circulation near the walls, especially in the column with a 10 µm sparger pore size (Fig.6a). The stronger liquid circulation led to more bubble travelling from the central core to the walls. It was resulted a sharp gas hold up profile and non-uniform distribution of the bubbles in the column with a 10 µm sparger pore size (Fig.6b)

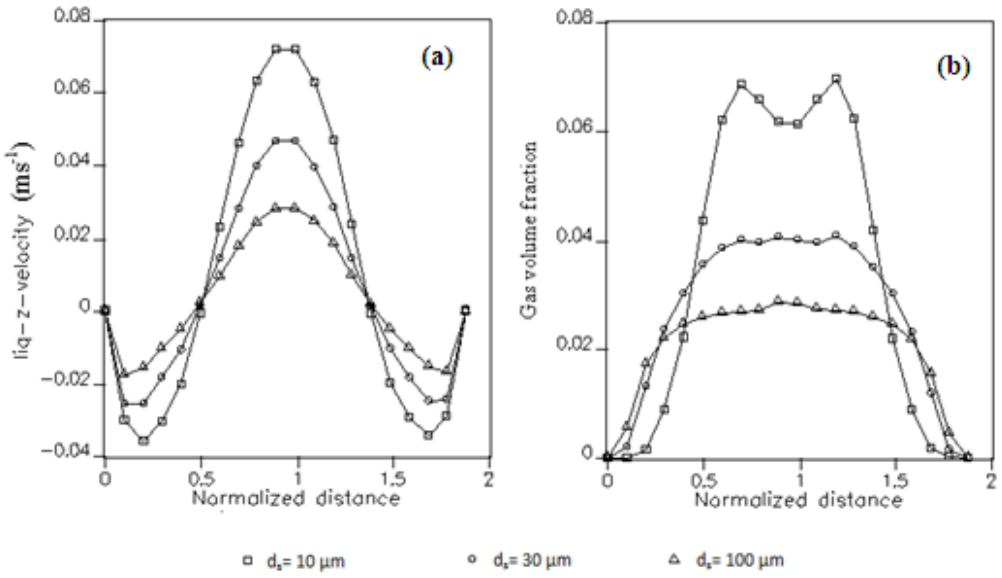


Fig. 6: a) Liquid z- velocity graphs at different pore sizes of spargers; b) Gas volume fraction profiles at different pore sizes of spargers. All graphs were obtained at the central x-z plane, superficial gas velocity of 0.003 m.s^{-1} and 5 s simulating.

By decreasing the sparger pore size, more number of the small bubbles entered in the column at a defined velocity and the volume fraction of gas increased subsequently. It was resulted in increased $K_L a$. In the column with smaller pore size of the sparger. The values of average bubble diameter, bubble rising velocity, gas hold up and $K_L a$ for different spargers at the superficial gas velocity of 0.003 m.s^{-1} have been shown in Table 2.

Table 2: Average bubble diameter, bubble rising velocity, gas hold up and $K_L a$ values for different sparger pore sizes.

Sparger pore size (µm)	d_b [(1)](×10^{-3}m)	u_b [(2)](m.s^{-1})	α_G	$K_L a$ [(3)](s^{-1})
100	0.81	0.43	0.021	0.033
30	0.61	0.48	0.027	0.069
10	0.42	0.58	0.032	0.13

(1) d_b is the average amount of bubble diameter calculated from equations (15) and (16)

(2) u_b is calculated from equation (14)

(3) $K_L a$ is predicted by CFD simulations according to equations (20) and (21).

3.6. Validation of the model

To prove the validity of the model, $K_L a$ was compared with the experimental data presented by Doig et al., [16] at different superficial gas velocities. Fig. (7a-b), shows a comparison between the model

prediction and the experimental data of $K_L a$, for the spargers with 30 and 100 μm pore sizes, respectively.

By increasing the superficial gas velocity, $K_L a$ increased as similar trend as experimental data. Fig. (7a) suggestes a good agreement between predicted $K_L a$ and the experimental results; however in the Fig. (7b), the simulation results were not close enough to the experimental data.

Applying constant and average bubble diameter in the simulations, assumed to be the main reason of observed differences in Fig. (7b). Use the micro pore size spargers practically increase the formation of chain bubbles, practically increase forming the chain of small bubbles, especially in higher superficial gas velocities. Coalescences caused by the chaining may be non-stable and break apart, but it is not negligible because of the small height and diameter of the column The existence of coalescence bubbles with different diameters in the experiment conditions, will be result in a decrease in the average gas hold up, bubble rising velocity and $K_L a$. Therefore the constant average bubble diameter applied to the model was not suitable enough to support the experimental data of the sparger with 100 μm pore size. Applying different classes of the bubble size to the model with considering the coalescence and break-up, may improve the obtained results.

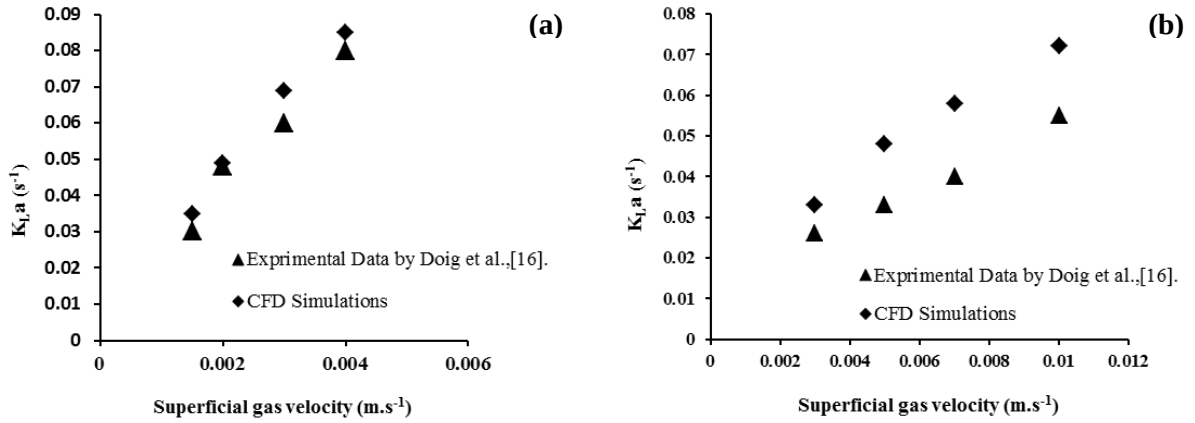


Fig. 7: Comparison the predicted $K_L a$ from the simulations and the experimental data for different spargers pore size; a and b are 30 and 100 μm sparger pore size, respectively.

4. Conclusions

Computational fluid dynamics is used to simulate the hydrodynamics behaviour in a MBCR for the first time. The results showed that CFD is a proper tool to predict the flow regime and $K_L a$ in this work. Applying a "RNG" $k-\varepsilon$ turbulent model with low turbulence intensity (0.05%) depicted the stable profiles in the simulations. The predicted $K_L a$ showed a good agreement with experimental

data presented by Doig et al., [16] for the column with a 30 μm sparger pore size in this work. Liquid circulation, gas distribution and their relation in the MBCR were as the same as the short bubble columns with an aspect ratio lower than 1.0. Observation the similar trend in the hydrodynamic characteristics of traditional and miniature scales of the bubble columns can encourage the researchers to design the miniature bioreactors besides the lab scales and develop the industrial bioprocesses using high-throughput systems.

Acknowledgments

The authors gratefully acknowledge the financial support of Biotechnology Development Council of Islamic Republic of Iran (project Number: TMU88-8-66).

References

[1] Islam RS, Tisi D, Levy MS, Lye GJ. Scale-up of Escherichia coli growth and recombinant protein expression conditions from microwell to laboratory and pilot scale based on matched k_La. *Biotechnology and Bioengineering.* 2008;99:1128-39.

[2] Kostov Y, Harms P, Randers-Eichhorn L, Rao G. Low-cost microbioreactor for high-throughput bioprocessing. *Biotechnology and Bioengineering.* 2001;72:346-52.

[3] Funke M, Diederichs S, Kensy F, Müller C, Büchs J. The baffled microtiter plate: Increased oxygen transfer and improved online monitoring in small scale fermentations. *Biotechnology and Bioengineering.* 2009;103:1118-28.

[4] Doig SD, Diep A, Baganz F. Characterisation of a novel miniaturised bubble column bioreactor for high throughput cell cultivation. *Biochemical Engineering Journal*. 2005;23:97-105.

[5] Merchuk JC, Ben-Zvi S, Niranjan K. Why use bubble-column bioreactors? *Trends in Biotechnology.* 1994;12:501-11.

[6] Kantarci N, Borak F, Ulgen KO. Bubble column reactors. *Process Biochemistry.* 2005;40:2263-83.

[7] Betts JI, Baganz F. Miniature bioreactors: Current practices and future opportunities. *Microbial Cell Factories.* 2006;5:21-35.

[8] Dhotre MT, Ekambara K, Joshi JB. CFD simulation of sparger design and height to diameter ratio on gas hold-up profiles in bubble column reactors. *Experimental Thermal and Fluid Science.* 2004;28:407-21.

[9] Olmos E, Gentric C, Vial C, Wild G, Midoux N. Numerical simulation of multiphase flow in bubble column reactors. Influence of bubble coalescence and break-up. *Chemical Engineering Science.* 2001;56:6359-65.

[10] Ekambara K, Dhotre MT, Joshi JB. CFD simulations of bubble column reactors: 1D, 2D and 3D approach. *Chemical Engineering Science.* 2005;60:6733-46.

[11] Darmana D, Deen NG, Kuipers JAM. Detailed modeling of hydrodynamics, mass transfer and chemical reactions in a bubble column using a discrete bubble model. *Chemical Engineering Science.* 2005;60:3383-404.

[12] Dhaouadi H, Poncin S, Hornut JM, Midoux N. Gas-liquid mass transfer in bubble column reactor: Analytical solution and experimental confirmation. *Chemical Engineering and Processing: Process Intensification.* 2008;47:548-56.

[13] Lamping SR, Zhang H, Allen B, Ayazi Shamlou P. Design ofa prototype miniature bioreactor for high throughput automated bioprocessing. *Chemical Engineering Science.* 2003;57:747-58.

[14] Zhang H, Lamping SR, Pickering SCR, Lye GJ, Shamlou PA. Engineering characterisation of a single well from 24-well and 96-well microtitre plates. *Biochemical Engineering Journal.* 2008;40:138-49.

[15] Rihani R, Guerri O, Legrand J. Three dimensional CFD simulations of gas-liquid flow in milli torus reactor without agitation. *Chemical Engineering and Processing: Process Intensification.* 2011;50:369-76.

[16] Doig SD, Ortiz-Ochoa K, Ward JM, Baganz F. Characterization of oxygen transfer in miniature and lab-scale bubble column bioreactors and comparison of microbial growth performance based on constant k_La. *Biotechnology Progress.* 2005;21:1175-82.

[17] Li G, Yang X, Dai G. CFD simulation of effects of the configuration of gas distributors on gas-liquid flow and mixing in a bubble column. *Chemical Engineering Science.* 2009;64:5104-16.

[18] Zhang T, Wei C, Feng C, Zhu J. A novel airlift reactor enhanced by funnel internals and hydrodynamics prediction by the CFD method. *Bioresource Technology.* 2012;104:600-7.

[19] Doran PM. Bioprocess engineering principles. first ed. London: Academic press; 1995.

[20] Krishna R, van Baten JM. Mass transfer in bubble columns. Catalysis Today. 2003;79-80:67-75.

[21] Monahan SM, Vitankar VS, Fox RO. CFD predictions for flow-regime transitions in bubble columns. *AIChE Journal.* 2005;51:1897-923.

[22] Bhavaraju SM, Russell TWF, Blanch HW. The design of gas sparged devices for viscous liquid systems. *AIChE Journal.* 1978;24:454-66.

[23] Sokolichin A, Eigenberger G. Applicability of the standard k-ε turbulence model to the dynamic simulation of bubble columns: Part I. Detailed numerical simulations. *Chemical Engineering Science.* 1999;54:2273-84.

[24] Yakhot V, Orszag SA, Thangam S, Gatski TB, Speziale CG. Development of turbulence models for shear flows by a double expansion technique. *Physics of Fluids A.* 1992;4:1510-21.

[25] Fluent A. Fluent 6.3 Users Guide. Fluent Inc. 2006.

[26] Ruzicka MC, Zahradník J, Drahoš J, Thomas NH. Homogeneous-heterogeneous regime transition in bubble columns. *Chemical Engineering Science.* 2001;56:4609-26.

[27] Sokolichin A, Eigenberger G, Lapin A, Lŭbert A. Dynamic numerical simulation of gas-liquid two-phase flows Euler/Euler versus Euler/Lagrange. *Chemical Engineering Science.* 1997;52:611-26.

[28] Delnoij E, Kuipers JAM, van Swaaij WPM. Computational fluid dynamics applied to gas-liquid contactors. *Chemical Engineering Science.* 1997;52:3623-38.

[29] Mudde RF, Simonin O. Two- and three-dimensional simulations of a bubble plume using a two-fluid model. *Chemical Engineering Science.* 1999;54:5061-9.

[30] Krishna R, van Baten JM. Eulerian simulations of bubble columns operating at elevated pressures in the churn turbulent flow regime. *Chemical Engineering Science.* 2001;56:6249-58.

[31] Sokolichin A, Eigenberger G, Lapin A. Simulation of buoyancy driven bubbly flow: Established simplifications and open questions. *AIChE Journal.* 2004;50:24-45.

[32] Delnoij E, Lammers FA, Kuipers JAM, van Swaaij WPM. Dynamic simulation of dispersed gas-liquid two-phase flow using a discrete bubble model. *Chemical Engineering Science.* 1997;52:1429-58.

[33] Silva MK, d'Ávila MA, Mori M. Study of the interfacial forces and turbulence models in a bubble column. *Computers and Chemical Engineering.* 2012;44:34-44.

[34] Delnoij E, Kuipers JAM, van Swaaij WPM. Dynamic simulation of gas-liquid two-phase flow: effect of column aspect ratio on the flow structure. *Chemical Engineering Science.* 1997;52:3759-72.

[35] Mousavi SM, Jafari A, Yaghmaei S, Vossoughi M, Turunen I. Experiments and CFD simulation of ferrous biooxidation in a bubble column bioreactor. *Computers & Chemical Engineering.* 2008;32:1681-8.

[36] Wiemann D, Mewes D. Calculation of flow fields in two and three-phase bubble columns considering mass transfer. *Chemical Engineering Science.* 2005;60:6085-93.

[37] Gopal JS, Sharma MM. Mass transfer characteristics of low H/D bubble columns. *The Canadian Journal of Chemical Engineering.* 1983;61:517-26.

[38] Ravinath M, Kasat GR, Pandit AB. Mixing Time in a Short Bubble Column. T*he Canadian Journal of Chemical Engineering.* 2003;81:185-95.

[39] Bahadori F, Rahimi R. Simulations of Gas Distributors in the Design of Shallow Bubble Column Reactors. *Chemical Engineering & Technology.* 2007;30:443-7.

[40] Buwa VV, Ranade VV. Dynamics of gas-liquid flow in a rectangular bubble column: experiments and single/multi-group CFD simulations. *Chemical Engineering Science.* 2002;57:4715-36.